Macromolecules

ARTICLE

pubs.acs.org/Macromolecules

Ethylene Copolymers with Crystallizable Side Chains

Miroslav Janicek,[*,†] Roman Cermak,[†,‡] Martin Obadal,[§] Christian Piel,[§] and Petr Ponizil[‡,⊥]

[†]Faculty of Technology, Department of Polymer Engineering, Tomas Bata University in Zlin, nam. T. G. Masaryka 275, 762 72 Zlin, Czech Republic

[‡]University Institute, Centre of Polymer Systems, Tomas Bata University in Zlin, Nad Ovcirnou 3658, 760 01 Zlin, Czech Republic

[§]Borealis Polyolefine GmbH, St. Peter Strasse 25, 4021 Linz, Austria

[⊥]Faculty of Technology, Department of Physics and Material Engineering, Tomas Bata University in Zlin, nam. T. G. Masaryka 275, 762 72 Zlin, Czech Republic

ABSTRACT: Metallocene-catalyzed copolymers of ethylene and α-olefins were investigated by X-ray scattering and differential scanning calorimetry. Evaluated α-olefin comonomers consisted of 8, 12, 18, or 26 carbons. As indicated from the small-angle X-ray scattering, ethylene−hexacosene copolymer with comonomer content of 3 mol % may contain second crystallites. Because no other reflections were observed in the wide-angle X-ray scattering patterns, the side-chain crystallites should have the same crystal lattice dimensions as the prevailing main-chain crystallites. Since this potential side chains crystallization can only be found in the ethylene−hexacosene copolymer with 3 mol % of comonomer, a critical concentration of long-chain comonomer should be reached for this secondary crystallite formation. It was also found that the thickness of the interlamellar amorphous layer stays virtually constant regardless of the changes in comonomer content and side-chain length.

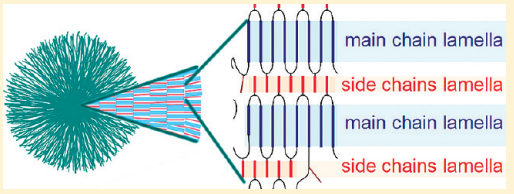

INTRODUCTION

Linear low-density polyethylene (LLDPE) is a copolymer of ethylene with small percentage of but-1-ene, hex-1-ene, or oct-1-ene, which represents a significant portion of 60 million tons worldwide annual production of polyethylenes (PE).[1] LLDPE could be produced using Ziegler−Natta catalysts, resulting in random comonomer distribution in the main chain.[2−4] On the other hand, metallocene catalysts can provide regular comonomer distribution, since the metallocene supramolecular structure enable tailoring of the macromolecule configuration.[5−8] Although these catalysts were broadly studied and applied primarily in polymerization of stereoregular polypropylene,[8−12] they were also successfully used for copolymerization of LLDPE.[6]

Kaminsky et al.[5] showed that cocatalyst system based on zirconocene and methylaluminoxane (MAO) is very active system for the copolymerization of ethylene and oct-1-ene. This zirconocene/MAO was used to prepare several ethylene-α-olefin copolymers where the oct-1-ene, dodec-1-ene, octadec-1-ene, and hexacos-1-ene were used as comonomers. Obtained LLDPEs had regular side-chains distribution along the main chain, and their properties were subject to study elsewhere.[5,13−16]

It is commonly known that the macroscopic properties of polyolefins strongly depend on the chain structure, and therefore, the quality of PE in both molten and solid state could be tuned by presence of side chains of various lengths and quantities. This dependence is caused by steric hindrances of the side chains what affects primarily the polymer crystallinity.[5,7] Generally agreed models also suppose that the side chains are incorporated in the amorphous phase, and only a small portion of the side-chain atoms are located inside crystalline regions, where they create packing errors.[13] On the contrary, Piel et al.[16] suggested that in some cases these short chains, namely those based on rather long comonomers, can crystallize and possibly create separated aggregates. The present article directs attention to assess the presence of second crystalline phase using X-ray scattering (both the wide-angle and small-angle setup) and differential scanning calorimetry (DSC).

EXPERIMENTAL SECTION

Materials. Copolymers of ethylene with oct-1-ene, dodec-1-ene, octadec-1-ene, and hexacos-1-ene as a comonomer were synthesized by a technique outlined elsewhere.[15−17] They are here denoted according to the comonomer length (the number following the letter "C") and the initial comonomer concentration (mol %) in a polymerization mixture (the number preceding the letter "C"), which fairly corresponds to the 1.5 and 3.0 mol % comonomer concentration in the macromolecule when comonomer conversion is considered. An overview of the copolymers and their previously published characteristics[15−17] is given in Table 1, where the reference ethylene homopolymer is denoted as L-PE.

Differential Scanning Calorimetry. The investigation of thermal behavior was done using a Perkin-Elmer Pyris 1 DSC power-compensated instrument calibrated with indium (T_m = 156.6 °C). About 6−8 mg of each sample was closed in an aluminum pan and measured with an empty pan as a reference. All measurements were initiated by rapid heating (50 K min^{-1}) from room temperature (20 °C) to 160 °C. At this temperature

Received: May 4, 2011
Revised: July 29, 2011
Published: August 17, 2011

Table 1. Ethylene Copolymers Characteristics and Branching Information Calculated from NMR and DSC Data by Piel et al.[16,17]

				DSC			NMR	
	M_w [kg mol^{-1}]	MWD	comonomer conv[a] [%]	T_m [°C]	T_c [°C]	x_c [%]	MSL[b] (bonds)	MSL[c] [Å]
L-PE	368	2.13	N/A	139.0	115.6	65.6	N/A	N/A
15C8	321	2.19	10.1	115.2	100.6	41.3	120	151.2
15C12	316	2.05	8.8	116.5	100.2	40.5	128	161.3
15C18	328	2.08	8.8	116.5	102.9	41.3	134	168.8
15C26	352	2.22	7.1	118.7	99.7	42.9	140	176.4
30C8	269	2.02	8.8	103.3	85.4	31.3	55	69.3
30C12	280	1.94	7.3	103.3	86.1	31.1	47	59.2
30C18	276	1.98	9.8	104.1	86.9	30.0	50	63.0
30C26	334	2.00	7.7	103.3	85.9	40.2	49	61.7

[a] Portion of the initial comonomer content incorporated into the macromolecule. [b] Methylene sequence length − the number of C−C bonds. [c] Methylene sequence length recalculated in Å; (MSL [Å] = (MSL[bonds]/2) × 2.52).

the samples were kept isothermally for 5 min. Afterward, they were cooled with rate −10 K min^{-1} down to 20 °C, and after 5 min of settling the material was heated with the same rate (10 K min^{-1}) back to 160 °C. All the measurements were performed under nitrogen as a purge constantly passing (20 mL min^{-1}) the DSC cells.

The values of each enthalpy change (ΔH_m) were gained using the instrument software, and they were recalculated using eq 1 to estimate crystallinity (x_c) of each material.

$$x_c = \frac{\Delta H_m}{\Delta H_m^0} \times 100\ [\%] \tag{1}$$

The heat of fusion of fully crystallized PE ($\Delta H_m^0 = 290$ J g^{-1}) was taken from the value listed in previous publications.[16,17]

Lamellar thickness (L_c) can be estimated from the position of a melting peak maximum by employing the Gibbs−Thomson equation (2) and the Flory equation (3).

$$T_m = T_m^c\left(1 - \frac{2\sigma_e}{\Delta H_u L_c}\right) \tag{2}$$

$$\frac{1}{T_m^c} = \frac{1}{T_m^0} - \frac{R}{\Delta H_u}\ln X_e \tag{3}$$

T_m is a melting temperature (maximum of melting peak), T_m^c stands for a copolymer melting temperature, X_e is a molar fraction of ethylene comonomer (for homopolymer $X_e = 1$), $T_m^0 = 418.6$ K represents an equilibrium melting temperature of PE, $\Delta H_u = 2.96 \times 10^8$ J m^{-3} is a volumetric heat of fusion, $\sigma_e = 0.09$ J m^{-2} represents a basal surface free energy, and $R = 8.314$ Pa m^3 K^{-1} mol^{-1} is a molar gas constant. The relation between X_e and T_m (eq 4) originates from curve fitting published elsewhere.[16]

$$\ln X_e = 0.331 - \frac{135.5}{T_m} \tag{4}$$

Sample Preparation for X-ray Scattering and Electron Microscopy. All the samples were subjected to recrystallization under controlled thermal conditions with a Perkin-Elmer DSC instrument. The specimens were in a shape of discs of 4 mm in diameter and thickness of ∼1 mm. They were placed in open DSC pans into both sample cells of the DSC apparatus simultaneously. Then heating from room temperature (20 °C) up to 160 °C was done with rate of 50 K min^{-1}. In the molten state, the materials were held for 5 min before cooling was performed with rate of −1 K min^{-1}. Specimens were cooled down to ambient temperature (20 °C). Subsequently, these specimens were used for X-ray diffraction studies directly, while for the scanning electron microscopy (SEM) the surface was additionally treated at room temperature by chemical etching in 1 wt % solution of $KMnO_4$ in 86% H_2SO_4 for 15 min. After washing in running water (10 min), specimens were washed in acetone and sputter-coated with Pd/Au alloy.

Scanning Electron Microscopy. A FEI Quanta FEG scanning electron microscope was used for the observation of the etched specimen surfaces; the Everhart-Thornley detector and 5 kV accelerated voltage were employed.

X-ray Scattering. Small-angle X-ray scattering (SAXS) was performed using a Molecular Metrology SAXS System with a pinhole camera attached to a microfocused X-ray beam generator (Osmic MicroMax-002) operating at 45 kV and 0.66 mA (30 W). The camera was equipped with a multiwire, gas-filled area detector with an active area diameter of 20 cm (Gabriel design). Two experimental setups were used to cover the scattering vector q in range of 0.005−1.1 Å^{-1}. The scattering intensities were put on an absolute scale using a glassy carbon standard. Additionally, the spectrum of the 30C26 copolymer was fit with a convolution curve of two peaks, which were calculated by means of iterative method using Pearson VII function.

To measure wide-angle X-ray scattering (WAXS) of the DSC-recrystallized samples a Bruker D8 Discover was used. The diffractometer was equipped with an X-ray tube with a copper target operating at 30 kV and 30 mA and a GADDS 2-D detector. To direct the beam on the surface, point-collimation (0.5 mm) was used. The measurement was done in reflection geometry, and 2θ angle was in the range from 11° to 32.5°. Data were collected for 300 s. Mathematical functions were used for fitting of individual intensity vs 2θ curves using TOPAS software (Bruker) to describe the amorphous and crystalline curves. The crystallinity index (X_c) was subsequently calculated from eq 5, where I_c and I_a are intensities of crystalline and amorphous phase, respectively, expressed by the area under WAXS curve.

$$X_c = \frac{I_c}{I_c + I_a} \times 100\ [\%] \tag{5}$$

RESULTS AND DISCUSSION

Differential Scanning Calorimetry. Table 2 summarizes crystallinity values obtained from eq 1. The characteristic temperatures (T_c and T_m) are the peak maxima shown in Figures 1 and 2. It is clear that the temperatures of transitions of the L-PE are the highest as compared to the rest of the samples (copolymers). This indicates better evolution of ordered structures in L-PE which is also confirmed by its highest x_c.

The dependences of the crystallinity index on the length of comonomer are plotted in Figure 3. Calculating from the heat of crystallization, only slight variation of the crystallinity can be seen

Table 2. Recorded and Evaluated DSC Data

	crystallization			melting			
	T_c [°C]	ΔH_c [J g^{-1}]	x_c [%]	T_m [°C]	ΔH_m [J g^{-1}]	x_c [%]	L_c [Å]
L-PE	116.0	157.9	54.4	135.0	170.6	58.8	241.3
15C8	99.6	71.4	24.6	113.2	86.4	29.8	78.7
15C12	100.3	76.8	26.5	113.2	90.2	31.1	78.7
15C18	102.1	83.0	28.6	114.2	91.3	31.5	81.2
15C26	100.4	75.3	26.0	115.0	76.4	26.3	83.3
30C8	85.3	72.5	25.0	99.7	58.4	20.1	55.5
30C12	86.1	56.5	19.5	100.5	65.1	22.4	56.5
30C18	85.7	58.3	20.1	102.6	54.7	18.9	59.3
30C26 major peak	85.9	54.6	18.8	101.0	58.0	20.0	57.2
30C26 minor peak				49.0	6.0		26.3

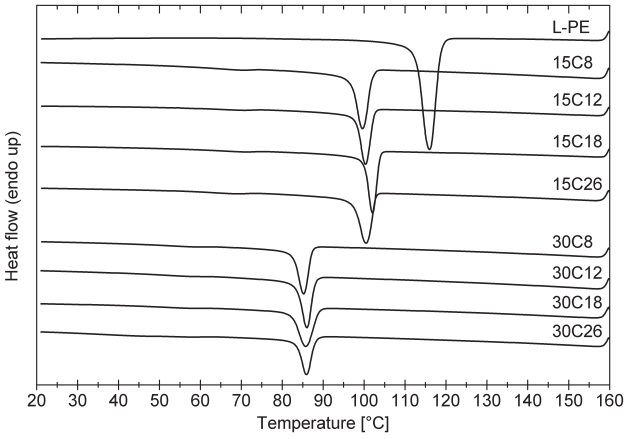

Figure 1. Comparison of cooling records. Curves are shifted vertically to better distinguish.

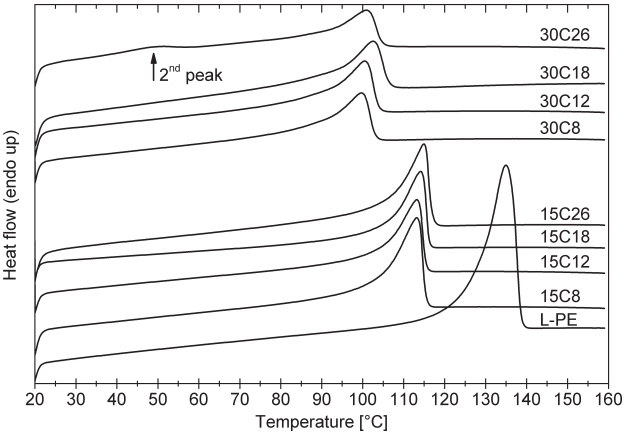

Figure 2. Comparison of heating records. Curves are shifted vertically to better distinguish; the second peak in 30C26 record is marked.

in 15C8, 15C12, 15C18, and 15C26. In the set of samples with higher content of side chains the 30C8 shows the highest crystallinity. The other samples, i.e., 30C12, 30C18, and 30C26, display nearly identical values. The values calculated from the heat of fusion show similar dependence for the copolymers with lower content of side chains. However, for

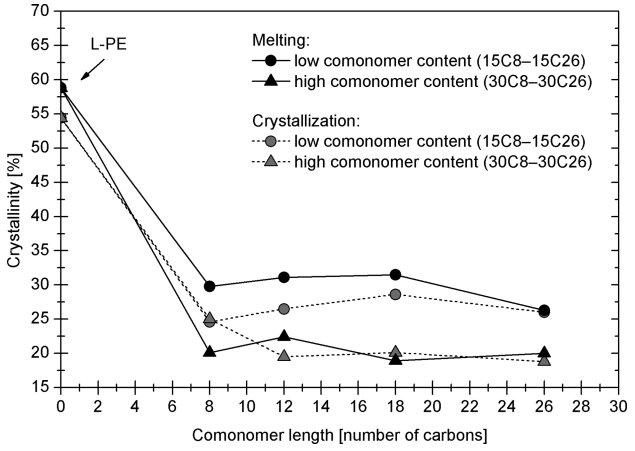

Figure 3. Crystallinity dependence on comonomer length. Values calculated using the heat of fusion and heat of crystallization.

the copolymers with more side chains the crystallinity nonmonotonically varies. As expected, the crystallinity indexes and melting/crystallization temperatures for the copolymers with higher content of side chains are always below those with lower side chains content.

In the DSC record (Figures 1 and 2) no second peak could be observed for any sample except for 30C26. This peak at $T_m = 49$ °C represents heat of ~6 J g^{-1}. It is worth noting that the pure hexacosene wax shows two melting peaks—at 37.3 and 52.6 °C—and the investigated copolymer was purified by repeated recrystallization to eliminate any erroneous signals.[16] As a consequence, the revealed peak should be ascribed to the polymer transition.

Wide-Angle X-ray Scattering. Table 3 shows the peak positions of the (110) and (200) reflections of all samples. As can be seen, the position of these maxima in case of L-PE is above all the values obtained for the copolymers. This implies that the distance between reflection planes is smaller (according to Bragg's law) when compared to other samples. As mentioned before, we cannot assume that all the side chains will be excluded from the crystalline regions and also Stadler et al.[18] admit the presence of side chains inside the crystallites, which widens the crystal lattice. On the other hand, they suppose that the short side chains will be most likely present in the lattice in comparison with longer side chains, which should remain outside the crystalline

dx.doi.org/10.1021/ma201017m |Macromolecules 2011, 44, 6759–6766

Table 3. Peak Positions in X-ray Patterns and Recalculated Material Characteristics

	peak position 2θ [deg]						
	(110)	(200)	X_c [%]	q_{max} [Å^{-1}]	LP [Å]	l_c [Å]	l_a [Å]
L-PE	21.537	23.906	73	0.013 57	463	338	125
15C8	21.432	23.715	48	0.036 90	170	82	88
15C12	21.432	23.715	48	0.035 51	177	85	92
15C18	21.432	23.732	51	0.032 88	191	97	94
15C26	21.415	23.732	55	0.032 88	191	104	87
30C8	21.327	23.593	35	0.046 48	135	47	88
30C12	21.310	23.575	36	0.044 72	141	51	90
30C18	21.310	23.523	40	0.039 85	158	63	95
30C26	21.362	23.506	46	0.032 88	191	88	103

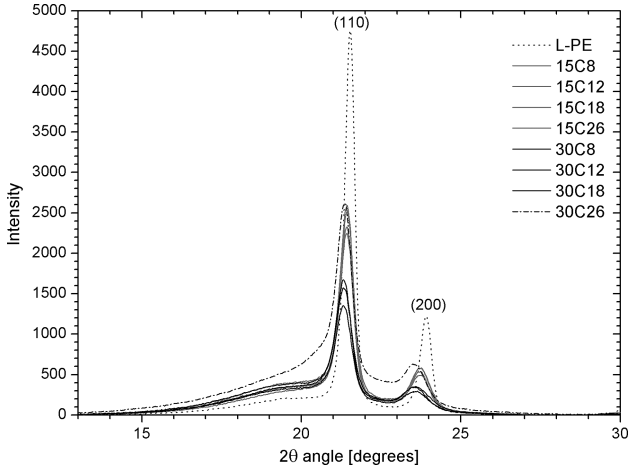

Figure 4. Summary of WAXS 1D spectra.

regions. These chains are then concentrated on the boundary of crystallites.

A considerable peak of L-PE points to the highest crystallinity index (X_c) if compared to all the other samples (Figure 4). Comparing copolymers with different comonomer amount −15C8 with 30C8, etc., it can be seen that both the 2θ angle and the crystallinity index are smaller for the samples with higher side chains content than the corresponding values for the samples with low number of side chains, which is in accordance with DSC data. The crystallinity index increases with the increasing comonomer chain length for both sets of samples (Figure 5). However, the WAXS-determined crystallinities are different from those calculated from the DSC as could arise from recrystallization effect during DSC measurement. In further text, the values mostly from X-ray scattering will be discussed.

Small-Angle X-ray Scattering. Figures 6 and 7 show Lorentz-corrected intensity vs scattering vector spectra. Expectably, the intensity maximum of L-PE points to the lowest scattering vector q of all measured samples, what refers to the biggest long period (LP), i.e., well-developed crystalline structure. The shoulder in the q range of 0.02−0.03 Å is a manifestation of a second peak hidden in the main peak. Deconvolution of this spectrum gives peaks with maxima at 0.0140 and 0.0287 Å^{-1}, which can be recalculated to LP of 449 and 224 Å, according to the Bragg's law (eq 6), where n is an integer which represents the order of

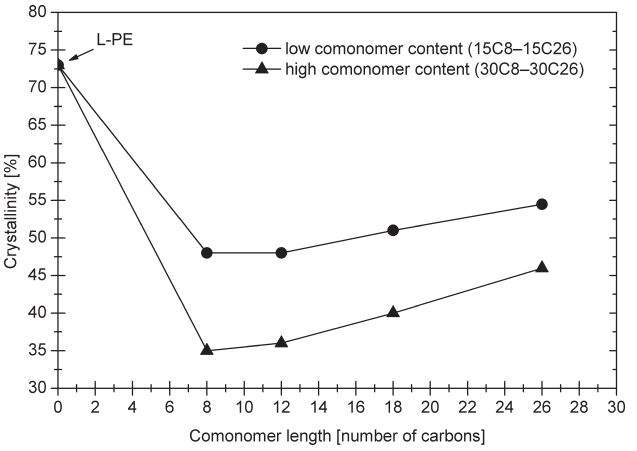

Figure 5. Crystallinity dependence on comonomer length. Values calculated from WAXS spectra.

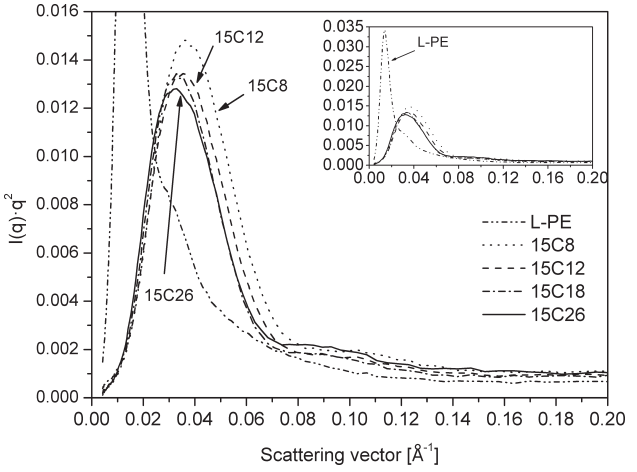

Figure 6. Lorentz-corrected SAXS patterns of homopolymer and samples with low comonomer content.

reflection. It is obvious the second peak is a second-order reflection.

$$\mathrm{LP} = \frac{2\pi n}{q} \tag{6}$$

Combining the WAXS and SAXS data (Table 3), we are able to estimate thicknesses of lamella (l_c) and amorphous layer (l_a). The relations are given by eqs 7 and 8.[19]

$$l_c = \frac{X_c}{100} \times \mathrm{LP} \tag{7}$$

$$\mathrm{LP} = l_c + l_a \tag{8}$$

Model. Figure 8 gives a summary of values of methylene sequence length (MSL) from nuclear magnetic resonance (NMR) data given by Piel et al.[16] compared to L_c, l_c, and l_a established in this paper. From the comparison of L_c and l_c with MSL, it is evident that the MSL values are higher than L_c or l_c for the low comonomer materials and that the MSLs are similar to L_c

dx.doi.org/10.1021/ma201017m |Macromolecules 2011, 44, 6759–6766

or l_c for the materials with higher comonomer content. This can be, particularly in the first case, explained by the entanglements restricting whole regular methylene sequences to be incorporated into lamellae within melt crystallization; also, the maximum lamellar thickness thermodynamically achievable at given crystallization conditions should be considered. It is worth noting that the length of the crystallizing sequences (from MSL, see Table 1) for the copolymer with 1.5 mol % of comonomer is nearly 1 time higher as compared to the relevant l_c in Table 3. As for the copolymers with higher comonomer content the values are similar. Even for the copolymer with lower comonomer content the length of crystallizing sequence does not allow to create two consecutive stems during lamellae formation. In both cases the lamellae should not be thus created via regular chain folding.

The phenomena described in the previous paragraph should certainly have an influence on the variation of amorphous layers. In the presented graph (Figure 8) the thickness of amorphous layer remains virtually constant within all copolymer samples. The same phenomenon was observed also by Nitta and Tanaka,[20] who have investigated primarily the dynamic mechanical properties of both metallocene-catalyzed linear PEs varying in weight-average molar mass (M_w) and copolymers of ethylene

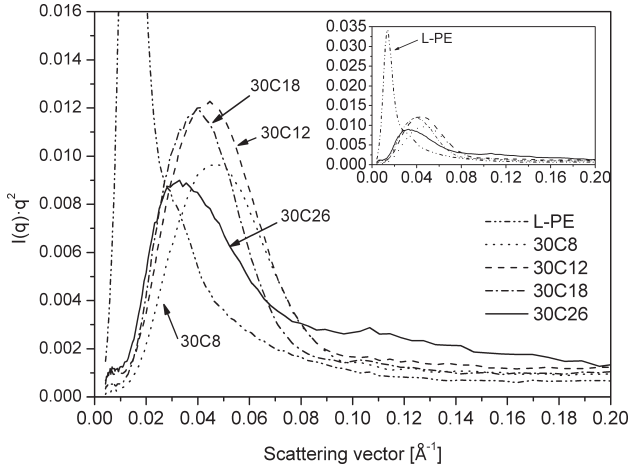

Figure 7. Lorentz-corrected SAXS patterns of homopolymer and samples with high comonomer content.

with 0.8−3.5 mol % of α-olefin as a comonomer. Beside the broad study of mechanical behavior, they investigated the crystalline structure by X-ray measurement. In the paper they stated that the thickness of amorphous layer is independent of the side chains amount. Stadler et al.[18] investigated the crystal lattice dimensions within the broad sample set prepared via both metallocene and Ziegler−Natta copolymerization where the comonomers were α-olefins of different lengths (4−26 carbons) and with different concentration of the comonomer. Concerning the l_a dependences, Stadler et al. found that the amorphous layer is widening with increase in M_w. Even though there was presented a fitting curve which describes the relation between l_a and the molar fraction of the comonomer, the influence of side chain length on the l_a was not investigated. Focusing on the l_a values in the present paper, it is obvious that the amorphous layer thickness is also independent of the side chains length. It can be presumed that the l_a value could be driven primarily by the M_w.

The l_c calculated from the SAXS/WAXS data for 30C26 sample is significantly higher than the others in the set of copolymers with 3.0 mol % of comonomer (Figure 8). The explanation of this phenomenon could be that the calculated thickness of the main chain lamellae is increased by the thickness of the lamellae created by the side chains. The maximum lamellar thickness of side chains lamella is the length of straighten chain—approximately 30 Å. Regarding the DSC data, the secondary peak in thermogram of 30C26 points lamellar thickness of 26.3 Å, which is in accordance with previously stated. If this length is subtracted from the calculated length of 88 Å, the overestimation is eliminated and the value fits with the others in the set. Moreover, the peak in the SAXS spectrum of 30C26 was found asymmetrical (Figure 7); thus, the deconvolution into two peaks was done by means of an iterative method (Figure 9). The positions of the individual peaks then pointed to LP of 194 and 122 Å, which means l_c is equal to 89 and 56 Å. This implies that in some cases the side chains can crystallize in the way that their thickness is added to the thickness of main-chain lamellae.

A model comprising two structures of crystalline regions could be proposed. In the material, there should be regions where the crystallites are created solely by main chain lamellae and the side chains are in an amorphous stay and regions where the side chains create crystallites on the surface of main chain lamellae. As no other diffraction peaks are seen in the WAXS record, we

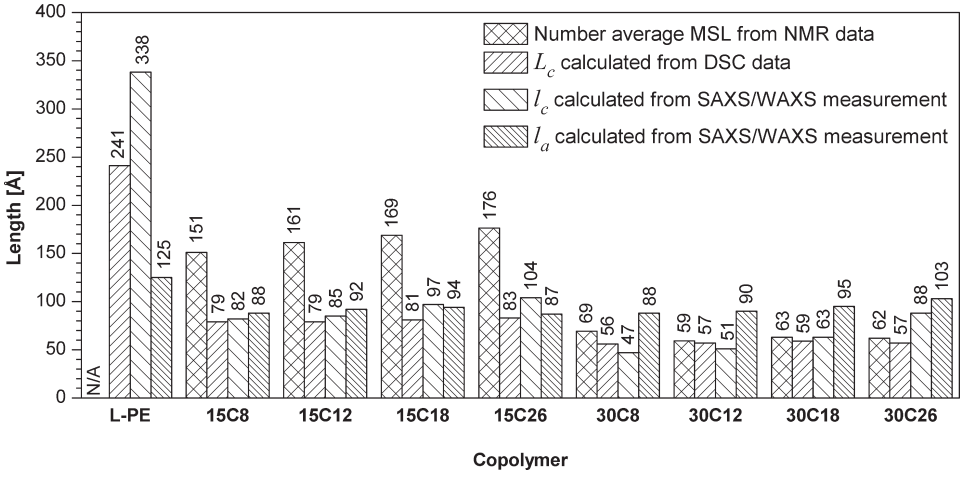

Figure 8. Comparison of number-average MSL calculated from NMR spectra[16] with L_c calculated from DSC data and l_c and l_a calculated from SAXS/WAXS measurement.

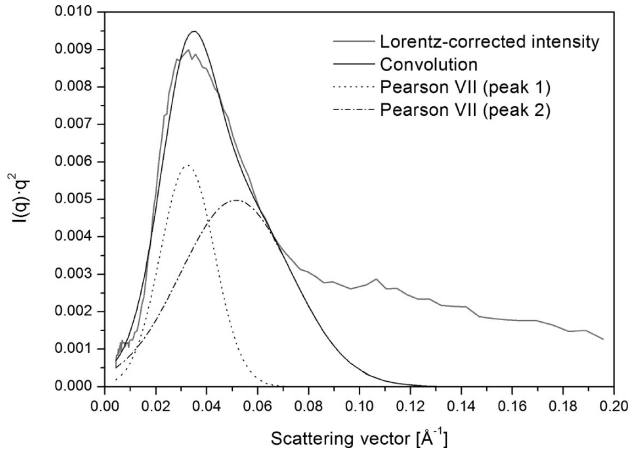

Figure 9. Deconvolution of the 30C26 SAXS spectrum with two peaks described by the Pearson VII function.

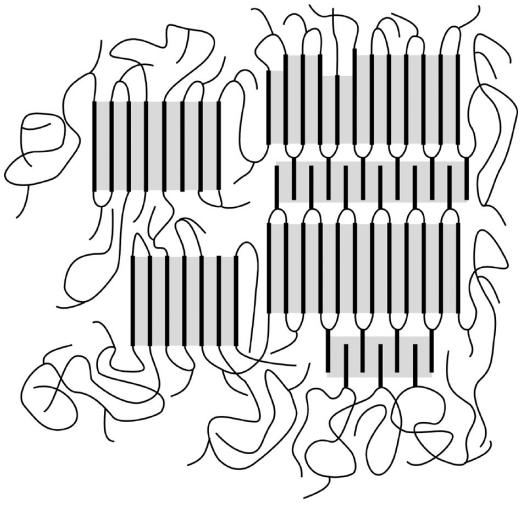

Figure 10. Idealized model of the folded chain with excluded branches on the lamella surface, which are in amorphous state (left) and crystallized (right).

suppose the side chains are crystallizing in the same crystal lattice dimensions as the main chain. An idealized model is given in Figure 10.

Since the second crystallites were proved only within the 30C26 sample, two main criteria for their formation can be stated: they are the comonomer length and concentration. The sufficient length is necessary to form initial nuclei while the concentration is needed both to have enough of chains to crystallize and to have enough of crystallites to get a signal of detectable intensity. Both seem to be fulfilled only in case of the hexacosene copolymer with high comonomer content.

It is obvious that the values of MSL and L_c are similar for the materials with 3 mol % of a given comonomer. This implies that the side chains can be in higher concentration localized close to the vicinity of the primary lamellae. Consequently, a strict spatial localization of the side chains can be supportive to their interaction and nucleation and overall crystallization.

Figure 11 shows SEM pictures of the homopolymer and hexacosene copolymer of both values of comonomer content. It should be pointed out that all previous discussions can only be considered if the materials crystallize into the lamellar morphology. To verify this point, scanning electron microscopy was employed showing clearly the formation of lamellar textures. The

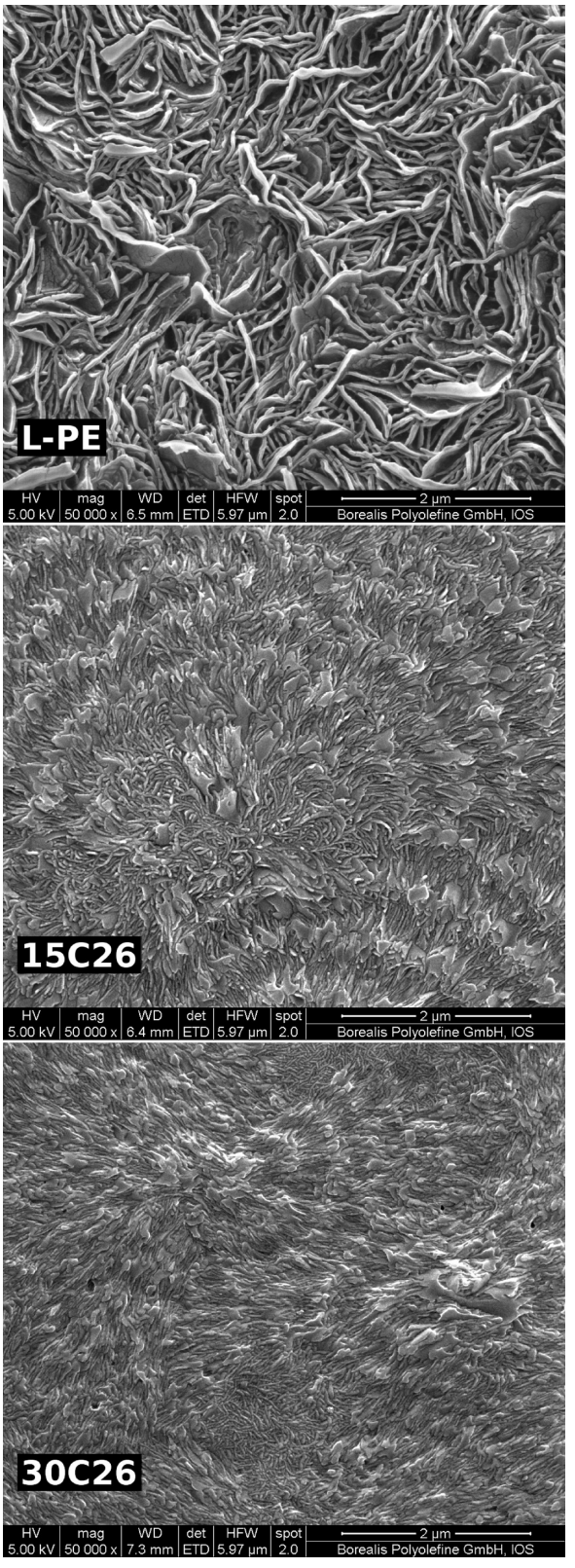

Figure 11. SEM pictures of the homopolymer and hexacosene copolymers, both low and high comonomer content.

dx.doi.org/10.1021/ma201017m |*Macromolecules* 2011, 44, 6759–6766

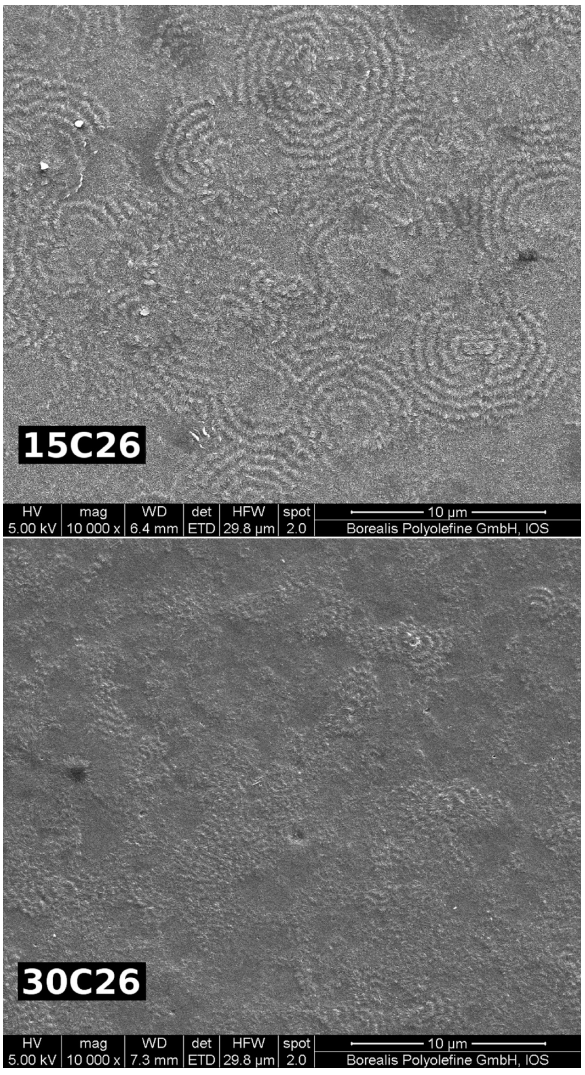

Figure 12. SEM pictures of the hexacosene copolymers, both low and high comonomer content, with lower magnification.

lamellar thickness is obviously reduced with the increasing comonomer content. However, in comparison with the SAXS data, the lamellae are thicker as might be related to the effects arising from the etching or metal sputtering. The SEM analysis is therefore used here in terms of qualitative assessment only. Unlike L-PE, the copolymers tend to form spherulites consisting of twisted lamellae; however, this effect is reduced again with further increasing comonomer amount. While in the material with lower comonomer content the lamellae are predominantly twisted, the 30C26 material consists of two distinctly different lamellar textures (cf. Figure 12). This might be related with the second maximum in the SAXS spectrum. Nevertheless, the existence of side chains lamellae in 30C26 cannot be unambiguously confirmed by SEM.

CONCLUSION

In the presented paper, we have studied the morphology of metallocene-catalyzed copolymers of ethylene and different α-olefins as a comonomer. These α-olefins were namely oct-1-ene, dodec-1-ene, octadec-1-ene, and hexacos-1-ene which provided copolymers with different side-chain lengths. Two sets of materials were studied: one with comonomer content ~1.5 mol % and the other with ~3.0 mol %. The aim was to prove whether the side chains are able to crystallize separately to the main-chain crystallites. DSC measurements gave evidence of secondary crystalline structures in the case of the hexacosene copolymer with high comonomer content, while the WAXS pattern pointed out that these structures have the same crystal lattice size as the prevailing crystallites. Data derived from the X-ray diffraction indicated the second crystalline structures in a size expected for the side chains lamellae. As the evidence of secondary crystallization was given only for the hexacosene copolymer with high comonomer content, two main criteria driving the potential side-chain crystals formation can be discussed; the side chain length and the side chains concentration should be high enough to let crystallization initiate and proceed. A sufficient amount of the side chains and its specific localization close to the primary lamellae are needed both to have enough crystallizable material and to create enough of crystallites to detect them. Regarding the interlamellar amorphous layer thickness estimated by the combination of SAXS and WAXS data, we have found it relatively constant regardless the side-chains length and the comonomer concentration.

AUTHOR INFORMATION

Corresponding Author

*E-mail: mjanicek@ft.utb.cz.

ACKNOWLEDGMENT

We thank Dr. Senthil K. Kaliappan of Borealis Polyolefine GmbH for WAXS measurements and to Dr. Gottfried Kandioller of Borealis Polyolefine GmbH for SEM pictures. The work was supported by the Operational Programme Research and Development for Innovations cofunded by the European Regional Development Fund (ERDF) and national budget of Czech Republic within the framework of the Centre of Polymer Systems project (reg. no.: CZ.1.05/2.1.00/03.0111). Miroslav Janicek gratefully acknowledges the financial support of this work by the internal grant of TBU in Zlin, No. IGA/11/FT/11/D, funded from the resources of specific university research.

REFERENCES

(1) Rojas, G.; Berda, E. B.; Wagener, K. B. *Polymer* **2008**, *49*, 2985–2995.
(2) Hernandez, R. J. Plastics in Packaging. In *Handbook of Plastics, Elastomers & Composites*; Harper, C. A., Ed.; McGraw-Hill Professional: New York, 2002.
(3) Abu-Sharkh, B.; Hussein, I. H. *Polymer* **2002**, *43*, 6333–6340.
(4) Zhang, M.; Lynch, D. T.; Wanke, S. E. *Polymer* **2001**, *42*, 3067–3075.
(5) Kaminsky, W.; Piel, C. *J. Mol. Catal. A: Chem.* **2004**, *213*, 15–19.
(6) Kaminsky, W. *Macromol. Chem. Phys.* **1996**, *197*, 3907–3945.
(7) Klimke, K.; Parkinson, M.; Piel, C.; Kaminsky, W.; Spiess, H. W.; Wilhelm, M. *Macromol. Chem. Phys.* **2006**, *207*, 382–395.
(8) Kaminsky, W. *Catal. Today* **1994**, *20*, 257–271.
(9) Shamshoum, E. S.; Rauscher, D. New Approaches for Ziegler-Natta Catalysts for Polypropylene. In *Metallocene-Catalyzed Polymers — Materials, Properties, Processing and Markets*. Benedikt, G. M., Goodall, B. L., Eds.; Plastics Design Library: Norwich, 1998.
(10) Kaminsky, W.; Hopf, A.; Piel, C. *J. Organomet. Chem.* **2003**, *684*, 200–205.
(11) Gómez-Elvira, J. M.; Tiemblo, P.; Elvira, M.; Matisova-Rychla, L.; Rychly, J. *Polym. Degrad. Stab.* **2004**, *85*, 873–882.
(12) Razavi, A.; Thewalt, U. *Coord. Chem. Rev.* **2006**, *250*, 155–169.

(13) Stadler, F. J.; Takahashi, T.; Yonetake, K. *e-Polym.* **2009**, 40.
(14) Stadler, F. J.; Piel, C.; Klimke, K.; Kaschta, J.; Parkinson, M.; Wilhelm, M.; Kaminsky, W.; Münstedt, H. *Macromolecules* **2006**, *39*, 1474–1482.
(15) Piel, C.; Stadler, F. J.; Kaschta, J.; Rulhoff, S.; Münstedt, H.; Kaminsky, W. *Macromol. Chem. Phys.* **2006**, *207*, 26–38.
(16) Piel, C.; Starck, P.; Seppälä, J. V.; Kaminsky, W. *J. Polym. Sci., Polym. Chem.* **2006**, *44*, 1600–1612.
(17) Piel, C. Polymerization of Ethene and Ethene-co-alpha-Olefin: Investigations on Short- and Long-Chain Branching and Structure-Property Relationships. Dissertation, Department of Chemistry, University of Hamburg, 2005.
(18) Stadler, F. J.; Takahashi, T.; Yonetake, K. *e-Polym.* **2009**, 41.
(19) Roe, R. J. Methods of X-Ray and Neutron Scattering in Polymer Science. In *Topics in Polymer Science*; Mark, J. E., Ed.; Oxford University Press: New York, 2000.
(20) Nitta, K.; Tanaka, A. *Polymer* **2001**, *42*, 1219–1226.